

www.acsaem.org Article

# Giant Manipulation of Phonon Hydrodynamics in Ferroelectric Bilayer Boron Nitride at Room Temperature and Beyond

Zhonghua Yang, Kunpeng Yuan, Nan Li, Xiaoliang Zhang, and Ming Hu\*



Cite This: ACS Appl. Energy Mater. 2022, 5, 8781–8790



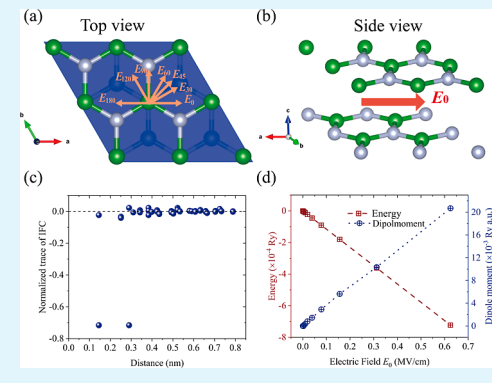
**ACCESS** 

III Metrics & More

Article Recommendations

s Supporting Information

**ABSTRACT:** Phonon hydrodynamics is an intriguing thermal transport mechanism that offers a great opportunity for phonon manipulation and thermal management. For decades, it has been believed that phonon hydrodynamics occurs only at very low temperatures, until very recently, it was confirmed that phonons can efficiently flow in low-dimensional materials at room temperature. However, to date, no study has been reported on the manipulation of phonon hydrodynamics at room temperature via reversible methods such as an external electric field. Motivated by the spontaneous out-of-plane polarization of ferroelectric bilayer boron nitride (BN), we investigate the effect of in-plane electric fields on phonon transport. With the electric field slightly switched on, the lattice thermal conductivity of bilayer BN steeply increases with a maximum augmentation factor of  $\sim$ 2, and the peak thermal conductivity reaches 840 W/mK. Such a colossal change stems from the dominant phonon hydrodynamics. By tuning the external



electric field, the phonon hydrodynamics can be manipulated to contribute 50% of the overall thermal transport in bilayer BN even at room temperature, indicating robust manipulation of phonon hydrodynamics. Over a broad frequency range (<10 THz), the Normal (N) phonon transport is 2 orders of magnitude stronger than that of the resistive Umklapp process. By analyzing mode level phonon behavior, we reveal that such enhancement is mainly contributed by the two low-frequency phonon branches (out-of-plane ZA and low-lying ZO<sub>1</sub>). Under the in-plane electric field, both the number of charges and charge distribution around the nitrogen atom can be largely altered, which is the natural response of the spontaneous electric polarization as a ferroelectric material, leading to phonon renormalization and modulation of phonon anharmonicity. Our study paves the way for dynamically controlling phonon hydrodynamics in layered ferroelectrics at room temperature and beyond without altering the atomic structure and would have a significant impact on emerging applications.

KEYWORDS: phonon hydrodynamics, ferroelectrics, thermal transport, first-principles, Boltzmann transport equation

## 1. INTRODUCTION

Exploring highly thermally conductive materials is of great importance to the disruptive development of micro-/nanoelectronics. The description of heat conduction in semiconductors and insulators has typically been based on Fourier diffusion theory. Over the past decades, a host of interesting phonon transport phenomena beyond the traditional Fourier diffusion picture have drawn much attention. Phonon hydrodynamics holds great promise for achieving high and controllable thermal transport, mainly due to the efficient "flow" of the Normal (N) phonon process in the materials overwhelming the resistive Umklapp (U) phonon process. Such Poiseuille flow of phonons has been observed by experiments in many materials, 3-7 where most scattering events conserve momentum and do not decay the heat flux. However, it has long been believed that phonon hydrodynamics occurs only at very low temperatures. Recently, some theoretical studies have suggested the presence of a strong Nprocess in low-dimensional materials near room temperature, such as two-dimensional (2D) graphene, 8,9 boron nitride (BN),<sup>7,10</sup> transition-metal dichalcogenides,<sup>11</sup> and one-dimensional ultra-thin Si nanowires<sup>12</sup> and single-walled carbon nanotubes.<sup>13</sup> Very rare cases were found in 3D bulk materials at relatively high temperatures. A special case was layered graphite,<sup>14–16</sup> both theoretically and experimentally confirmed. Therefore, it has remained a longstanding challenge to identify some materials where phonon hydrodynamics can take place at relatively high temperatures. A knottier problem that has not been reported so far is to find a robust way to control the phonon hydrodynamics.

Ferroelectric materials are dielectric materials in which polarization remains permanently, even after removing the applied electric field, and the direction of the dipole moment

Received: April 27, 2022 Accepted: July 4, 2022 Published: July 14, 2022





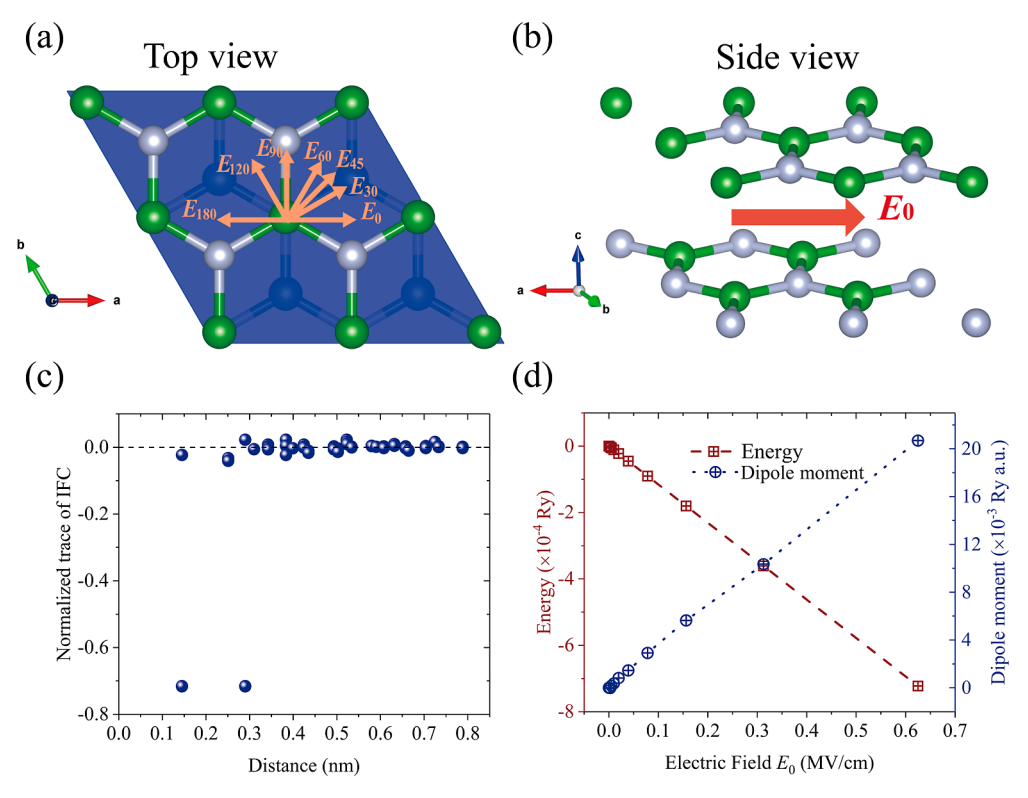


**Figure 1.** (a) Atomic structure of bilayer BN and the direction of the in-plane electric field. The gray (green) sphere represents a nitrogen (boron) atom. The subscript number of the electric field strength represents the angle between the in-plane electric field and the *a*-axis. (b) Side view of bilayer BN. The arrow indicates the horizontal (in-plane) electric field applied. (c) Normalized trace of interatomic force constant tensors vs atomic distances. (d) Energy (left-axis) and the dipole moment (right-axis) as a function of the electric field strength along the *a*-axis.

can be switched using an external electric field. Ferroelectric materials are technologically important for many applications. 17-20 2D materials are free of dangling bonds, offering merits such as high carrier mobility, 21 band gap tunability, 2 and structure flexibility.<sup>23</sup> So far, a large family of 2D layered materials have been experimentally confirmed or theoretically predicted as piezoelectric or ferroelectric,<sup>24</sup> such as monolayer transition-metal dichalcogenides,<sup>25</sup> group IV monochalcogenides,<sup>26–29</sup> and group III-V binary compounds.<sup>29–31</sup> BN can form a 2D structure with great similarity to graphene, which is an insulator with a wide band gap. 32-34 Layered hexagonal boron nitride is a wide-band-gap insulator and was theoretically predicted to possess planar piezoelectric properties.<sup>35</sup> More strikingly, for bilayer BN, a strong charge transfer from the top layer to the bottom layer induced by the closer interlayer B-N distance results in vertical spontaneous electric polarization,<sup>36</sup> which provides the possibility to tune its transport properties through an external electric field.

Traditional methods for modulating the lattice thermal conductivity ( $\kappa_{\rm L}$ ) in crystalline materials include doping, alloying, and chemical functionalization, which generally requires changing the atomic structure and thus are irreversible. Electric field is a noncontact and friendly method that is reversible, requiring no alteration of the atomic structure. Some 2D layered materials display a spontaneous vertical (out-of-plane) electric polarization, offering promise for tunable  $\kappa_{\rm L}$  by applying horizontal (in-plane) electric fields. Motivated by the nature of ferroelectricity, we apply an inplane electric field to influence the interatomic electrostatic interaction and finally manipulate the phonon transport in bilayer BN. In this paper, we demonstrate that phonon hydrodynamics contribute significantly to the overall thermal

transport in bilayer BN at room temperature, and such inherent phonon hydrodynamics is very sensitive to external electric fields. The fundamental insight into the influence of an electric field on the N phonon scattering process is analyzed from the microscopic view of the phonon behaviors and the electronic structure. Our study provides solid evidence for robustly modulating phonon hydrodynamics in low-dimensional ferroelectric materials at room temperature by applying an external electric field with strength achievable in experiments, which is expected to have a broad impact on practical applications of ferroelectrics.

#### 2. METHODS

DFT calculations were performed with the Quantum ESPRESSO (QE) package<sup>37</sup> with the SSSP Precision pseudopotentials.<sup>38,39</sup> The kinetic energy cutoff for wavefunctions is set to 80 Ry. A mesh grid of  $24 \times 24 \times 1$  in the first Brillouin zone (BZ) is adopted, and the total electron energy convergence threshold for self-consistency is 1 × 10<sup>-10</sup> Ry and the crystal lattice is fully relaxed with a force-threshold of  $1 \times 10^{-7}$  Ry/Bohr and a vacuum spacing of 20 Å along the out-ofplane direction. The thickness of bilayer BN is chosen as 6.66 Å for the  $\kappa_{\rm L}$  calculation. The second- and third-order interatomic force constants (IFCs) were calculated using the finite displacement approach<sup>42</sup> with 5 × 5 × 1 supercells for all cases. The phonon dispersions were calculated using the PHONOPY package.<sup>43</sup> The third-order IFC calculations were truncated at the fifth nearest neighbors. We calculated the  $\kappa_L$  by solving the phonon Boltzmann transport equation (BTE) iteratively as implemented in the ShengBTE package.<sup>44</sup> The convergence of the cutoff radius of anharmonic IFCs should be tested.<sup>45</sup> We quantify the strength of interatomic interactions by calculating the normalized trace of IFC tensors.<sup>46</sup> This parameter indicates how a large cutoff radius should be used to evaluate the anharmonic IFCs by effectively including the possibly strong interaction strength as revealed by the large trace

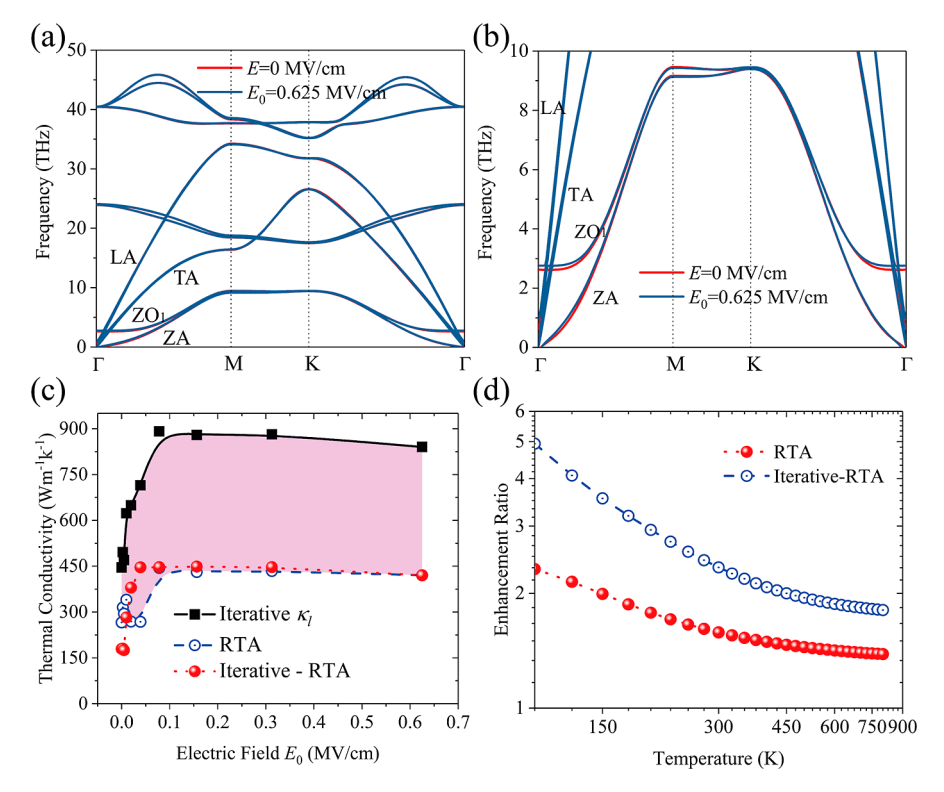


Figure 2. (a) Phonon dispersion of bilayer BN. (b) Zoom-in view of the low-frequency part of the phonon dispersion. (c) Influence of an electric field on the lattice thermal conductivity, where the electric field is applied along the a-axis. The shaded area denotes the contribution of phonon hydrodynamics. (d) Temperature-dependent enhancement ratio for pure resistive RTA  $\kappa_L$  and phonon hydrodynamics (difference between iterative  $\kappa_L$  and RTA result) under an electric field of 0.625 MV/cm with respect to a zero electric field.

value. There exist strong interactions between B and N atoms when the cutoff radius is less than 0.3628 nm (fifth nearest neighbors) (Figure 1c). Beyond that, the trace values are very weak, indicating negligible IFCs. We also test the convergence of the Q-grid. The  $\kappa_{\rm L}$  of bilayer BN is well-converged when the Q-grid is greater than  $51 \times 51$ × 1. In-plane electric fields with different strengths and directions are applied to tune the  $\kappa_L$  of bilayer BN (Figure 1a). No observable change in the  $\kappa_{\rm L}$  was found for out-of-plane electric fields with the same magnitude of strength. The electric field was applied based on the modern theory of polarization<sup>47,48</sup> as implemented in the QE package. With the strength of the electric field increasing, the energy of bilayer BN decreases, showing a more thermodynamically stable structure in the external electric field (Figure 1d). The dipole energy correction partially contributes to the decrease in energy due to the linearly increasing dipole moment with the electric field. A similar phenomenon was also observed in other 2D materials.<sup>49</sup>

## 3. RESULTS AND DISCUSSION

Figure 2a shows the phonon dispersion of bilayer BN. The unit cell of bilayer BN contains four atoms, resulting in three acoustic dispersion branches [XA, (X = L, T, and Z)] and nine optical dispersion branches (XO). The longitudinal acoustic (LA) and transverse acoustic (TA) branches correspond to inplane vibration, while the other one (ZA) corresponds to out-of-plane vibration. The LA and TA modes show a linear dependence on the wave vector near the BZ, while the ZA mode exhibits a quadratic dispersion, which is very similar to those found in monolayer and layered systems. Figure 2b shows a partially enlarged view of phonon dispersion by comparing a zero electric field and 0.625 MV/cm. The phonon dispersions with and without electric fields are very similar. The only exceptions are the ZA and ZO<sub>1</sub> modes, which exhibit slight differences. As we all know, the phonon group velocity is

determined by the slope of the dispersion relation  $v = \partial \omega / \partial q$ . Therefore, a slight increase of phonon group velocity of ZA could be observed. To verify the difference in the group velocity of bilayer BN with and without an electric field, the phonon modes vibrating along the out-of-plane direction (ZA) are selected according to their eigenvectors, and the corresponding phonon frequency and group velocity are shown in Figure S1 of the Supporting Information. It is found that the group velocity of ZA under 0.625 MV/cm is larger than that of the zero electric field, especially in the lower frequency range (<4THz), which is quite in accord with the phonon frequency in Figure 2a,b. To gain insight into the changes of the phonon group velocity more deeply, we apply force on the bond length of B-N (see the inset of Figure S1 of the Supporting Information for illustration). We notice a slight decrease in the bond length of the in-plane B-N bond by 0.02% caused by the electric field of 0.625 MV/cm. Typically, the decrease in the bond length leads to the enhancement of the phonon group velocity; a similar conclusion is also obtained in the previous literature.<sup>53</sup> The above observation suggests that the ZA and ZO<sub>1</sub> modes may play a dominant role in the  $\kappa_L$  difference. As discussed later, the  $\kappa_L$  of bilayer BN is obviously lower than that of monolayer BN because the ZO<sub>1</sub> modes hybridize with the acoustic modes in the bilayer BN, which means more three-phonon processes, and thus results in lower phonon lifetimes.

Figure 2c shows the dependence of the  $\kappa_L$  of bilayer BN on the strength of the electric field. The  $\kappa_L$  at no electric field is calculated to be 445.8 W m<sup>-1</sup> K<sup>-1</sup>, which is consistent with a previous study. When the electric field along the *a*-axis is switched on, the  $\kappa_L$  first steeply increases and then remains at a plateau afterward. Under the electric field  $E_0 = 0.625$  MV/cm,

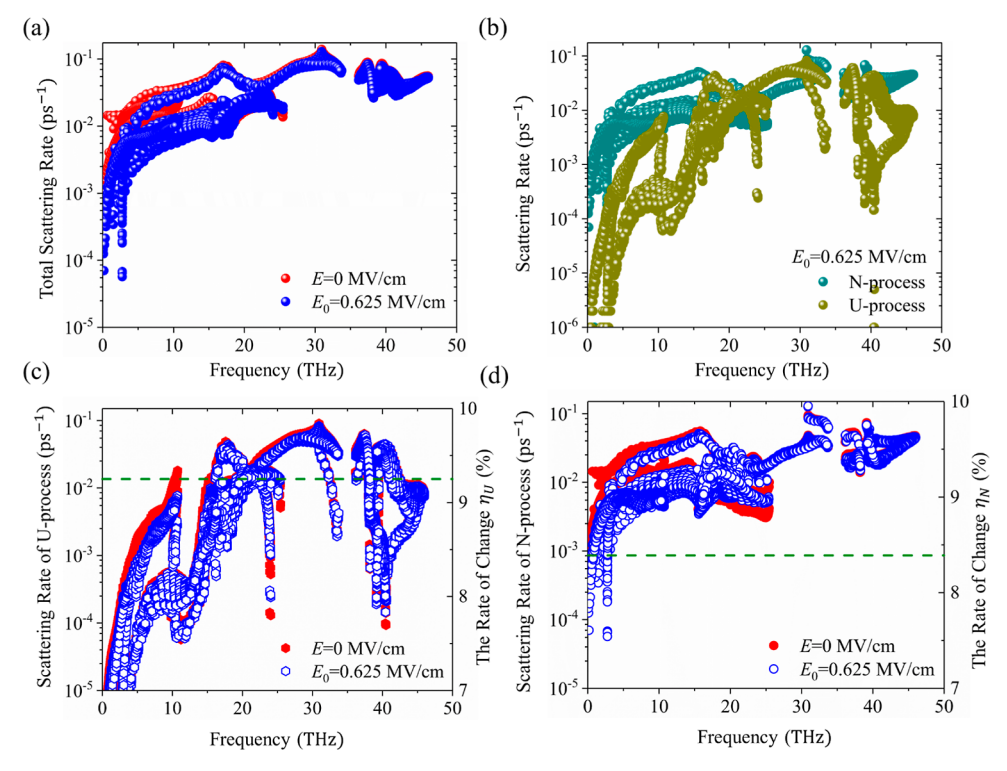


Figure 3. Comparison of the scattering rates at room temperature. (a) Total scattering rates without and with the electric field of 0.625 MV/cm. (b) N-process and U-process under an electric field of 0.625 MV/cm. (c) U-process and (d) N-process with respect to 0 and 0.625 MV/cm electric fields.

the  $\kappa_L$  of bilayer BN reaches an ultrahigh value of 840.4 W m<sup>-1</sup> K<sup>-1</sup>. Here, an augmentation factor is used to estimate the change rate of thermal conductivity with and without an electric field. For bilayer BN, the augmentation factor of thermal conductivity with a 0.625 MV/cm electric field is about ~1.9 times that of bilayer BN at no external electric field. In a recent study, a 5 MV/cm out-of-plane electric field was applied,<sup>53</sup> and the increase of the  $\kappa_L$  of bulk GaN is only ~12%. The  $\kappa_L$  of 2D silicene under an external electric field first increases and then decreases, and the maximum value under 0.9 MV/cm is 2.4 times that of the  $\kappa_L$  without an electric field.<sup>49</sup> In our previous work,<sup>50</sup> an extremely high external electric field (40 MV/cm) is required to obtain an obvious  $\kappa_{\rm L}$ change. Here, the relatively low electric field strength of 0.625 MV/cm, which is realizable in experiments,  $^{56}$  could tune the  $\kappa_{\rm L}$ of bilayer BN to a comparable change magnitude. This result is very promising for practical device applications.<sup>57</sup> It is also worth noting that the  $\kappa_L$  of bilayer BN at an electric field of 0.625 MV/cm is even higher than that for single-layer BN, which is calculated separately to be 704 W m<sup>-1</sup> K<sup>-1</sup> at room temperature. This is unusual considering that for layered materials with weak interlayer interactions, the in-plane  $\kappa_{\rm L}$ usually decreases as the number of layers increases.

More interestingly, for bilayer BN, the difference between the iterative  $\kappa_L$  and the single relaxation time approximation (RTA)  $\kappa_L$  (herein denoted as "iterative - RTA") increases tremendously as the electric field strength increases (Figure 2c). The  $\kappa_L$  difference with an electric field of 0.625 MV/cm is 2.34 times that without an electric field, indicating strong phonon hydrodynamics augmentation. The BTE is solved iteratively starting with a zeroth-order approximation,  $F_{\lambda^0} = \tau_{\lambda^0} V_{\lambda}$ , which corresponds to the RTA  $\kappa_L$ . The iterative process has a large impact on the results when N-processes play an

important role, as RTA deals with all phonon-phonon interactions as resistive. 14,44 Therefore, for bilayer BN, the difference between the iterative  $\kappa_L$  and RTA result increasing with the electric field means that the N-process becomes significant and even dominates the entire phonon transport, which is the signature of phonon hydrodynamics. Phonon hydrodynamics contribute 40% of overall thermal transport at no electric field, and the contribution increases to 50% for the electric field of 0.625 MV/cm. We also studied the effect of the orientation of the electric field on the  $\kappa_L$  for an electric field of 0.625 MV/cm. The  $\kappa_{\rm L}$  of bilayer BN reaches the lowest (667 W m<sup>-1</sup> K<sup>-1</sup>) when the electric field is rotated as 30° with respect to the a-axis, and the  $\kappa_L$  reaches the highest (926 W m<sup>-1</sup> K<sup>-1</sup>) when this angle becomes 120° (see Figure S3 of the Supporting Information), resulting in a degree of modulation of 40%. The oscillating behavior of the electric field orientation-dependent thermal conductivity indicates that the phonon transport in ferroelectric bilayer BN is very sensitive to the external electric field.

We categorized the three-phonon scattering process into an N-process and a U-process by judging whether the momentum conservation rule is obeyed, that is, k+k'-k''=0 (N-process) or k+k'-k''=G (U-process), where G is a nonzero reciprocal lattice vector. If the N-process is dominant in the three-phonon scattering, the out-of-equilibrium distributions can be redistributed by a strong N-process with quite a small reduction by the U-process, such that these corresponding phonon modes will have the same drift velocity and form a hydrodynamic phonon "fluid" flow. In the ultimate case, if the phonon scattering process is totally an N-process, the out-of-equilibrium distributions will never decay to the equilibrium state and thus will lead to an infinite  $\kappa_{\rm L}$  (divergence). For bilayer BN, the electric field enhances the total  $\kappa_{\rm L}$  of bilayer

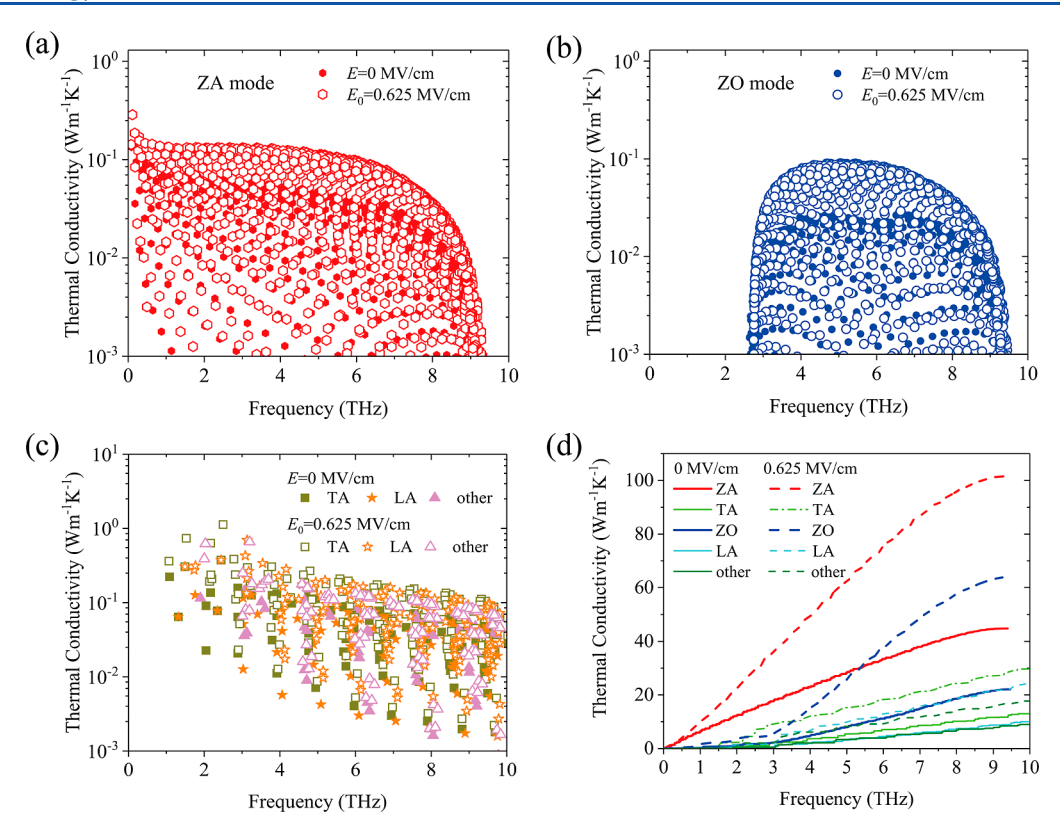


Figure 4. Contributions of (a) ZA, (b) ZO<sub>1</sub>, and (c) TA and LA and other phonon modes to the thermal conductivity under the electric fields of 0 and 0.625 MV/cm. (d) Comparison of frequency-dependent cumulative thermal conductivities for different phonon modes.

BN mainly due to the significantly augmented contribution from phonon hydrodynamics.

We first exclude the influence of the slight change in the phonon dispersions which define the group velocity (Figure 2b). Then, the major factor should come from the phonon lifetime according to the kinetic theory of phonon transport, that is,  $\kappa_{\rm L} \propto C v^2 \tau$ , where C, v, and  $\tau$  are the specific heat capacity, average phonon group velocity, and average phonon lifetime, respectively. Figure 3a clearly shows that at room temperature, the total phonon scattering rate of bilayer BN under an electric field of 0.625 MV/cm is lower than that without an electric field, especially in the low-frequency range (<10 THz), which results in a higher phonon lifetime and eventually a higher  $\kappa_L$  as shown in Figure 2c. For further insight into the dependence of the phonon scattering rate of bilayer BN on the strength of an electric field, the Grüneisen parameter is shown in Figure S2 of the Supporting Information, and we found that the absolute magnitude of the Grüneisen parameter decreases obviously when an electric field of 0.625 MV/cm is applied, which leads to a lower phonon scattering rate. We split the total scattering rate into the U-process and the N-process, shown in Figure 3b, and show a comparison of their scattering rate change in Figure 3c,d. The N- and U-process in the BTE solution was split by the PHONO3PY package.<sup>59</sup> It is found that the N-process is much stronger than the U-process  $(N_0/U_0 > 1)$  under a 0 MV/ cm electric field. Furthermore, when the electric field is switched on, the absolute reduction of the scattering rate of the N-process is far larger than that of the U-process, which leads to the decrease of the total phonon scattering rate of bilayer BN. To further quantitatively compare the relative changes of the two processes, the N-process and U-process scattering

rates were averaged and the change rates ( $\eta$ ) between 0 and 0.625 MV/cm electric fields are plotted by an olive dashed line, shown in Figure 3c,d. It is obvious that the influence of an electric field on the change rate of the U-process is higher than that of the N-process ( $\eta_{\rm N} < \eta_{\rm U}$ ). Since  $N_{0.625}/U_{0.625} = N_0/U_0 \times (1-\eta_{\rm N})/(1-\eta_{\rm U})$ , the N-process with a 0.625 MV/cm electric field would be stronger than that of the U-process, which is in accord with the results shown in Figure 3b. Compared to the 0 MV/cm electric field, the N-process would contribute more to the total scattering rate under a 0.625 MV/cm electric field, that is,  $N_{0.625}/U_{0.625} > N_0/U_0$ . This provides the evidence that the electric field enhances the  $\kappa_{\rm L}$  of bilayer BN by augmenting the phonon hydrodynamics.

To better understand the underlying mechanism, we plot the contribution of different phonon modes to  $\kappa_L$  with respect to frequency. In the dominant frequency range (<10 THz), there mainly exist three acoustic phonon branches (ZA, TA, and LA) and one optical branch (ZO<sub>1</sub>), and other phonon modes are defined as "other" in Figure 4c. Phonon modes at an electric field of 0.625 MV/cm contribute more to the total  $\kappa_L$ . Especially, the ZA and ZO<sub>1</sub> modes contribute the most, which is consistent with the difference shown in Figure 2b. We extracted the mode level  $\kappa_L$  of the ZA (Figure 4a) and ZO<sub>1</sub> (Figure 4b) modes. The ZA modes almost occupy the entire low-frequency range (<10 THz), while the ZO<sub>1</sub> modes only occupy the frequency range of 2.6-10 THz. These frequency ranges are in the same region where the N-process is strongly enhanced (Figure 3b). Combining Figures 3b and 4a,b evidently shows the tremendously boosted contribution of the N-process from ZA and ZO<sub>1</sub> modes to the overall thermal transport when an electric field is applied. The cumulative  $\kappa_{\rm L}$ with and without an electric field is also shown in Figure 4d.

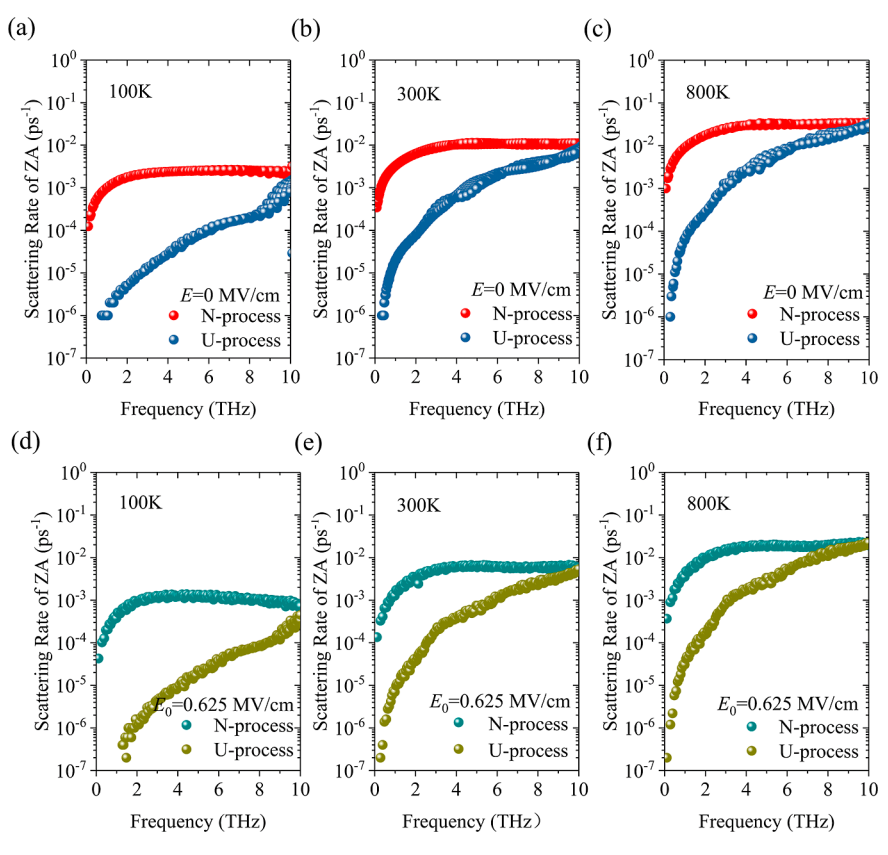


Figure 5. Temperature-dependent N and U phonon scattering rates from 100 to 800 K under (a-c) no electric field and a (d-f) 0.625 MV/cm electric field.

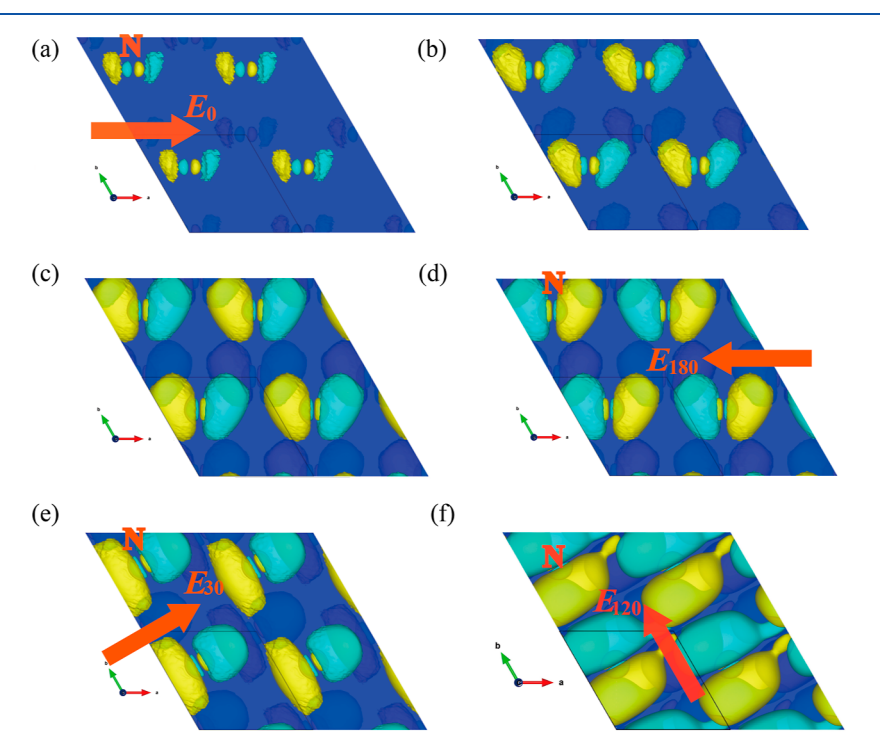


Figure 6. CDD under different strengths and directions of electric fields. (a)  $E_0 = 0.15625$  MV/cm. (b)  $E_0 = 0.3125$  MV/cm. (c)  $E_0 = 0.625$  MV/cm. (d)  $E_0 = -0.625$  MV/cm. (e)  $E_{30} = 0.625$  MV/cm. (f)  $E_{120} = 0.625$  MV/cm. The yellow and cyan isosurfaces correspond to positive and negative values of  $6.6 \times 10^{-5}$  a.u., respectively. The arrow indicates the direction of the electric field. The position of nitrogen atoms is labeled as "N".

We can more clearly obtain the underlying mechanism that (1) the influence of the electric field on the  $\kappa_L$  of ferroelectric

bilayer BN is mainly due to the ZA and  $ZO_1$  phonon modes since the absolute  $\kappa_L$  increase of these two types of phonon

modes is more evident and (2) for ZA modes, the influence happens in the entire low-frequency range (<10 THz), while for ZO<sub>1</sub> modes, the influence is concentrated in the range of 2.6-10 THz.

Most of the phonon hydrodynamics occurs at low temperatures such as < 1 K. Few materials were recently identified to exhibit phonon hydrodynamics at a much higher temperature. 16,60,61 This makes us wonder if the strong phonon hydrodynamics in bilayer BN will disappear at temperatures well above room temperature. In Figure 5, we show the N and U phonon scattering rates of ZA from 100 to 800 K under zero and 0.625 MV/cm electric fields. With temperature increasing, the scattering rates of the N-process and U-process go up, and the N-process is always much stronger than the U-process. Moreover, comparing the scattering rates under the same temperature, both the scattering rates of the N-process and U-process decrease when an electric field is applied, which is in accord with the results shown in Figure 3. We then compared the RTA  $\kappa_L$  and phonon hydrodynamics contribution with (0.625 MV/cm) and without an electric field. Their respective enhancement ratios are shown in Figure 2d. The electric field enhances the contribution of phonon hydrodynamics to the overall phonon transport more severely than RTA contribution throughout the entire temperature range studied (100-800 K). At room temperature, the electric field enhances the RTA  $\kappa_{\rm L}$  and phonon hydrodynamics by  $\sim$ 1.6 and  $\sim$ 2.3, respectively. These enhancement ratios persist to be  $\sim$ 1.4 and  $\sim$ 1.8, respectively, even if the temperature increases to 800 K. This indicates that the electric field can hold the phonon hydrodynamics in bilayer BN at a high level even at elevated temperatures. The result is exciting as an electric field can be utilized to tune the phonon hydrodynamics in bilayer BN for a wide range of working temperatures, which provides great promise for realistic device applications. We also studied quantitative dependence of phonon hydrodynamics on temperature and compared the results with single-layer BN and graphene (see Section 3 in the Supporting Information for details: temperature dependence of phonon hydrodynamics in bilayer BN).

Considering the inherent relationship between the phonon properties and interatomic electrostatic interaction, we further explore the underlying mechanism responsible for the electric field-modulated phonon hydrodynamics and phonon anharmonicity from the perspective of the electronic structure. The charge density difference (CDD) represents the charge redistribution due to external factors. The CDD caused by the electric field is calculated by  $\Delta \rho = \rho(E) - \rho(0)$ . Figure 6a-c shows the CDD of ferroelectric bilayer BN under electric fields of 0.15625, 0.3125, and 0.625 MV/cm along the positive a-axis, respectively. In contrast, if the electric field is exerted along the negative a-axis, the charge distribution will be opposite (Figure 6d). The charge polarization relies on the strength and direction of the external electric field. The charge moves in the opposite direction of the electric field.<sup>63</sup> In addition, the stronger the electric field, the more charges are induced, causing a higher  $\kappa_L$ , similar to the case of 2D silicene. 49 Since the direction of the electric field has a different effect on the  $\kappa_L$ , we also show the CDD under 30 and 120° electric fields in Figure 6e,f, respectively. The induced charge is also rotated, and the more charge around the N atom is induced by a 120° electric field, which in turn enhances the  $\kappa_{\rm L}$ obviously (see Figure S3 of the Supporting Information). Although it is challenging to quantitatively describe the difference of charge distribution in space, the above analysis evidently shows the variation of the charge environment felt by the N cores, which will renormalize the interactions around the N atom and is thus believed to have a consequent influence on the phonon anharmonicity and further the  $\kappa_{\rm L}$  of ferroelectric bilayer BN.

## 4. CONCLUSIONS

In summary, motivated by the inherent spontaneous out-ofplane polarization of ferroelectric bilayer BN, we comprehensively investigate the effect of in-plane electric fields on manipulating phonon hydrodynamic transport. Note that we take 0.625 MV/cm as a crucial electric field strength to discuss, which should be easy to realize in the experimental implementation. In recent experiments, the electric-fieldinduced thermal conductivity modulation has been observed in the ferroelectric materials. The electric field strength is in the range of 100-190 MV/cm and 250-280 MV/cm, which is more than 2 orders of magnitude stronger than the electric field in our work. At room temperature, the  $\kappa_{\rm L}$  of bilayer BN first dramatically increases with an increase in the strength of the electric field and then achieves a plateau. The overall  $\kappa_{\rm L}$ of bilayer BN steeply reaches the peak value with a corresponding augmentation factor of ~2 under a mild electric field strength of 0.625 MV/cm and can be modulated to be ~40% higher with the same electric field strength when carefully rotating the electric field by 30°. The reason that the  $\kappa_{\rm L}$  of bilayer BN is very sensitive to both the strength and orientation of the external electric field is that the external electric field can affect the phonon hydrodynamic transport (particularly for ZA and ZO<sub>1</sub> phonon modes) more severely than the U-process, leading to a significantly enhanced contribution from phonon hydrodynamics. A temperature dependence study confirms that the enhancement of phonon hydrodynamics can persist at elevated temperatures well above room temperature. We also provide the qualitative relationship between phonon transport characteristics and the interatomic electrostatic interaction. When an electric field is applied, more charges are induced around the nitrogen atoms, leading to phonon renormalization and the modulation of phonon anharmonicity through interatomic electrostatic interaction. Regarding the possibility of experimental implementation, the time-domain thermoreflectance technique could be used to measure the thermal transport properties under applied electric fields. 66-68 Therefore, the results gained from this work unveil a new route of manipulating phonon hydrodynamics in ferroelectric materials at room temperature and beyond without affecting atomic structures, which provide an important guidance for designing layered materials with dynamically controllable thermal transport properties.

## ASSOCIATED CONTENT

## Supporting Information

The Supporting Information is available free of charge at https://pubs.acs.org/doi/10.1021/acsaem.2c01274.

Electric field strength-dependent group velocity and Grüneisen parameter of bilayer BN; electric field orientation-dependent thermal conductivity of bilayer BN; and temperature-dependent phonon hydrodynamics in bilayer BN (PDF)

#### AUTHOR INFORMATION

### **Corresponding Authors**

Xiaoliang Zhang — Key Laboratory of Ocean Energy Utilization and Energy Conservation of Ministry of Education, School of Energy and Power Engineering, Dalian University of Technology, Dalian 116024, China; Email: zhangxiaoliang@dlut.edu.cn

Ming Hu — Department of Mechanical Engineering, University of South Carolina, Columbia 29208, USA; orcid.org/0000-0002-8209-0139; Email: hu@sc.edu

#### **Authors**

Zhonghua Yang — Department of Mechanical Engineering, University of South Carolina, Columbia 29208, USA; School of Architecture and Civil Engineering, Shenyang University of Technology, Shenyang 110870, China

Kunpeng Yuan – Key Laboratory of Ocean Energy Utilization and Energy Conservation of Ministry of Education, School of Energy and Power Engineering, Dalian University of Technology, Dalian 116024, China

Nan Li – School of Architecture and Civil Engineering, Shenyang University of Technology, Shenyang 110870, China

Complete contact information is available at: https://pubs.acs.org/10.1021/acsaem.2c01274

#### **Author Contributions**

These authors contributed equally to this work.

#### Notes

The authors declare no competing financial interest.

## ACKNOWLEDGMENTS

This project is supported by the Natural Science Foundation of Education Department of Liaoning Province (grant nos. LQGD2020008, 20180540122, 200005636, 200005720) and the National Natural Science Foundation of China [51720105007, 52076031, 51806031]. Z.Y. and K.Y. acknowledge the support from the China Scholarship Council. The research reported in this publication was supported in part by the NSF (award number 2030128).

## REFERENCES

- (1) Qian, X.; Zhou, J.; Chen, G. Phonon-engineered extreme thermal conductivity materials. *Nat. Mater.* **2021**, *20*, 1188–1202.
- (2) Chen, G. Non-Fourier phonon heat conduction at the microscale and nanoscale. *Nat. Rev. Phys.* **2021**, *3*, 555–569.
- (3) Glassbrenner, C. J.; Slack, G. A. Thermal Conductivity of Silicon and Germanium from 3°K to the Melting Point. *Phys. Rev.* **1964**, *134*, A1058–A1069.
- (4) Martelli, V.; Jiménez, J. L.; Continentino, M.; Baggio-Saitovitch, E.; Behnia, K. Thermal Transport and Phonon Hydrodynamics in Strontium Titanate. *Phys. Rev. Lett.* **2018**, *120*, 125901.
- (5) Sussmann, J. A.; Thellung, A. Thermal Conductivity of Perfect Dielectric Crystals in the Absence of Umklapp Processes. *Proc. Phys. Soc., London* **1963**, *81*, 1122–1130.
- (6) Guyer, R. A.; Krumhansl, J. A. Thermal Conductivity, Second Sound, and Phonon Hydrodynamic Phenomena in Nonmetallic Crystals. *Phys. Rev.* **1966**, *148*, *778*–788.
- (7) Cepellotti, A.; Fugallo, G.; Paulatto, L.; Lazzeri, M.; Mauri, F.; Marzari, N. Phonon hydrodynamics in two-dimensional materials. *Nat. Commun.* **2015**, *6*, 6400.
- (8) Narozhny, B. N.; Gornyi, I. V.; Titov, M. Anti-Poiseuille flow in neutral graphene. *Phys. Rev. B* **2021**, *104*, 075443.
- (9) Huang, X.; Lucas, A. Electron-phonon hydrodynamics. *Phys. Rev. B* **2021**, *103*, 155128.

- (10) Lee, S.; Broido, D.; Esfarjani, K.; Chen, G. Hydrodynamic phonon transport in suspended graphene. *Nat. Commun.* **2015**, *6*, 6290
- (11) Torres, P.; Alvarez, F. X.; Cartoixà, X.; Rurali, R. Thermal conductivity and phonon hydrodynamics in transition metal dichalcogenides from first-principles. 2D Materials 2019, 6, 035002.
- (12) Zhou, Y.; Zhang, X.; Hu, M. Nonmonotonic Diameter Dependence of Thermal Conductivity of Extremely Thin Si Nanowires: Competition between Hydrodynamic Phonon Flow and Boundary Scattering. *Nano Lett.* **2017**, *17*, 1269–1276.
- (13) Lee, S.; Lindsay, L. Hydrodynamic phonon drift and second sound in a (20,20) single-wall carbon nanotube. *Phys. Rev. B* **2017**, *95*, 184304
- (14) Ding, Z.; Zhou, J.; Song, B.; Chiloyan, V.; Li, M.; Liu, T.-H.; Chen, G. Phonon Hydrodynamic Heat Conduction and Knudsen Minimum in Graphite. *Nano Lett.* **2018**, *18*, 638–649.
- (15) Jeong, J.; Li, X.; Lee, S.; Shi, L.; Wang, Y. Transient Hydrodynamic Lattice Cooling by Picosecond Laser Irradiation of Graphite. *Phys. Rev. Lett.* **2021**, *127*, 085901.
- (16) Huberman, S.; Duncan, R. A.; Chen, K.; Song, B.; Chiloyan, V.; Ding, Z.; Maznev, A. A.; Chen, G.; Nelson, K. A. Observation of second sound in graphite at temperatures above 100 K. *Science* **2019**, 364, 375–379.
- (17) Kim, T. Y.; Kim, S. K.; Kim, S.-W. Application of ferroelectric materials for improving output power of energy harvesters. *Nano Convergence* **2018**, 5, 30.
- (18) Roy, A.; Gupta, R.; Garg, A. Multiferroic Memories. Adv. Condens. Matter Phys. 2012, 2012, 926290.
- (19) Martin, L. W.; Rappe, A. M. Thin-film ferroelectric materials and their applications. *Nat. Rev. Mater.* **2016**, *2*, 16087.
- (20) Wang, W.; Li, J.; Liu, H.; Ge, S. Advancing Versatile Ferroelectric Materials Toward Biomedical Applications. *Adv. Sci.* **2021**, *8*, 2003074.
- (21) Li, X.; Cai, W.; An, J.; Kim, S.; Nah, J.; Yang, D.; Piner, R.; Velamakanni, A.; Jung, I.; Tutuc, E.; Banerjee, S. K.; Colombo, L.; Ruoff, R. S. Large-Area Synthesis of High-Quality and Uniform Graphene Films on Copper Foils. *Science* **2009**, 324, 1312.
- (22) Keum, D. H.; Cho, S.; Kim, J. H.; Choe, D.-H.; Sung, H.-J.; Kan, M.; Kang, H.; Hwang, J.-Y.; Kim, S. W.; Yang, H.; Chang, K. J.; Lee, Y. H. Bandgap opening in few-layered monoclinic MoTe2. *Nat. Phys.* **2015**, *11*, 482–486.
- (23) Wu, W.; Wang, L.; Li, Y.; Zhang, F.; Lin, L.; Niu, S.; Chenet, D.; Zhang, X.; Hao, Y.; Heinz, T. F.; Hone, J.; Wang, Z. L. Piezoelectricity of single-atomic-layer MoS2 for energy conversion and piezotronics. *Nature* **2014**, *514*, 470–474.
- (24) Chen, X.; Li, W.; Diaz, A.; Li, Y.; Chen, Y.; McDowell, D. L. Recent progress in the concurrent atomistic-continuum method and its application in phonon transport. *MRS Commun.* **2017**, *7*, 785–797.
- (25) Duerloo, K.-A. N.; Ong, M. T.; Reed, E. J. Intrinsic Piezoelectricity in Two-Dimensional Materials. *J. Phys. Chem. Lett.* **2012**, *3*, 2871–2876.
- (26) Fei, R.; Kang, W.; Yang, L. Ferroelectricity and Phase Transitions in Monolayer Group-IV Monochalcogenides. *Phys. Rev. Lett.* **2016**, *117*, 097601.
- (27) Fei, R.; Li, W.; Li, J.; Yang, L. Giant piezoelectricity of monolayer group IV monochalcogenides: SnSe, SnS, GeSe, and GeS. *Appl. Phys. Lett.* **2015**, *107*, 173104.
- (28) Hu, T.; Dong, J. Two new phases of monolayer group-IV monochalcogenides and their piezoelectric properties. *Phys. Chem. Chem. Phys.* **2016**, *18*, 32514–32520.
- (29) Şahin, H.; Cahangirov, S.; Topsakal, M.; Bekaroglu, E.; Akturk, E.; Senger, R. T.; Ciraci, S. Monolayer honeycomb structures of group-IV elements and III-V binary compounds: First-principles calculations. *Phys. Rev. B* **2009**, *80*, 155453.
- (30) Blonsky, M. N.; Zhuang, H. L.; Singh, A. K.; Hennig, R. G. Ab Initio Prediction of Piezoelectricity in Two-Dimensional Materials. *ACS Nano* **2015**, *9*, 9885–9891.

- (31) Gao, R.; Gao, Y. Piezoelectricity in two-dimensional group III-V buckled honeycomb monolayers. *Phys. Status Solidi RRL* **2017**, *11*, 1600412.
- (32) Tian, Y.; Xu, B.; Yu, D.; Ma, Y.; Wang, Y.; Jiang, Y.; Hu, W.; Tang, C.; Gao, Y.; Luo, K.; Zhao, Z.; Wang, L.-M.; Wen, B.; He, J.; Liu, Z. Ultrahard nanotwinned cubic boron nitride. *Nature* **2013**, 493, 385–388.
- (33) Shi, Y.; Hamsen, C.; Jia, X.; Kim, K. K.; Reina, A.; Hofmann, M.; Hsu, A. L.; Zhang, K.; Li, H.; Juang, Z.-Y.; Dresselhaus, M. S.; Li, L.-J.; Kong, J. Synthesis of Few-Layer Hexagonal Boron Nitride Thin Film by Chemical Vapor Deposition. *Nano Lett.* **2010**, *10*, 4134–4139.
- (34) Li, X.; Zhao, J.; Yang, J. Semihydrogenated BN Sheet: A Promising Visible-light Driven Photocatalyst for Water Splitting. *Sci. Rep.* **2013**, *3*, 1858.
- (35) Michel, K. H.; Verberck, B. Theory of elastic and piezoelectric effects in two-dimensional hexagonal boron nitride. *Phys. Rev. B* **2009**, 80, 224301.
- (36) Li, L.; Wu, M. Binary Compound Bilayer and Multilayer with Vertical Polarizations: Two-Dimensional Ferroelectrics, Multiferroics, and Nanogenerators. *ACS Nano* **2017**, *11*, 6382–6388.
- (37) Giannozzi, P.; Baroni, S.; Bonini, N.; Calandra, M.; Car, R.; Cavazzoni, C.; Ceresoli, D.; Chiarotti, G. L.; Cococcioni, M.; Dabo, I.; Dal Corso, A.; de Gironcoli, S.; Fabris, S.; Fratesi, G.; Gebauer, R.; Gerstmann, U.; Gougoussis, C.; Kokalj, A.; Lazzeri, M.; Martin-Samos, L.; Marzari, N.; Mauri, F.; Mazzarello, R.; Paolini, S.; Pasquarello, A.; Paulatto, L.; Sbraccia, C.; Scandolo, S.; Sclauzero, G.; Seitsonen, A. P.; Smogunov, A.; Umari, P.; Wentzcovitch, R. M. QUANTUM ESPRESSO: a modular and open-source software project for quantum simulations of materials. *J. Phys.: Condens. Matter* **2009**, *21*, 395502.
- (38) Prandini, G.; Marrazzo, A.; Castelli, I. E.; Mounet, N.; Marzari, N. Precision and efficiency in solid-state pseudopotential calculations. *npj Comput. Mater.* **2018**, *4*, 72.
- (39) Lejaeghere, K.; Bihlmayer, G.; Björkman, T.; Blaha, P.; Blügel, S.; Blum, V.; Caliste, D.; Castelli, I. E.; Clark, S. J.; Dal Corso, A.; de Gironcoli, S.; Deutsch, T.; Dewhurst, J. K.; Di Marco, I.; Draxl, C.; Dułak, M.; Eriksson, O.; Flores-Livas, J. A.; Garrity, K. F.; Genovese, L.; Giannozzi, P.; Giantomassi, M.; Goedecker, S.; Gonze, X.; Grånäs, O.; Gross, E. K. U.; Gulans, A.; Gygi, F.; Hamann, D. R.; Hasnip, P. J.; Holzwarth, N. A. W.; Iuşan, D.; Jochym, D. B.; Jollet, F.; Jones, D.; Kresse, G.; Koepernik, K.; Küçükbenli, E.; Kvashnin, Y. O.; Locht, I. L. M.; Lubeck, S.; Marsman, M.; Marzari, N.; Nitzsche, U.; Nordström, L.; Ozaki, T.; Paulatto, L.; Pickard, C. J.; Poelmans, W.; Probert, M. I. J.; Refson, K.; Richter, M.; Rignanese, G.-M.; Saha, S.; Scheffler, M.; Schlipf, M.; Schwarz, K.; Sharma, S.; Tavazza, F.; Thunström, P.; Tkatchenko, A.; Torrent, M.; Vanderbilt, D.; van Setten, M. J.; Van Speybroeck, V.; Wills, J. M.; Yates, J. R.; Zhang, G.-X.; Cottenier, S. Reproducibility in density functional theory calculations of solids. Science 2016, 351, aad3000.
- (40) Yang, X.; Zhang, B. Twisted bilayer graphene/h-BN under impact of a nano-projectile. *Appl. Surf. Sci.* **2021**, *538*, 148030.
- (41) Paszkowicz, W.; Pelka, J. B.; Knapp, M.; Szyszko, T.; Podsiadlo, S. Lattice parameters and anisotropic thermal expansion of hexagonal boron nitride in the 10–297.5 K temperature range. *Appl. Phys. A: Solids Surf.* **2002**, *75*, 431–435.
- (42) Esfarjani, K.; Chen, G.; Stokes, H. T. Heat transport in silicon from first-principles calculations. *Phys. Rev. B* **2011**, *84*, 085204.
- (43) Togo, A.; Oba, F.; Tanaka, I. First-principles calculations of the ferroelastic transition between rutile-type and CaCl2-typeSiO2at high pressures. *Phys. Rev. B* **2008**, *78*, 134106.
- (44) Li, W.; Carrete, J.; Katcho, A.; Mingo, N. ShengBTE: A solver of the Boltzmann transport equation for phonons. *Comput. Phys. Commun.* **2014**, *185*, 1747–1758.
- (45) Qin, G.; Qin, Z.; Wang, H.; Hu, M. On the diversity in the thermal transport properties of graphene: A first-principles-benchmark study testing different exchange-correlation functionals. *Comput. Mater. Sci.* **2018**, *151*, 153–159.

- (46) Lee, S.; Esfarjani, K.; Luo, T.; Zhou, J.; Tian, Z.; Chen, G. Resonant bonding leads to low lattice thermal conductivity. *Nat. Commun.* **2014**, *5*, 3525.
- (47) Umari, P.; Pasquarello, A. Ab initioMolecular Dynamics in a Finite Homogeneous Electric Field. *Phys. Rev. Lett.* **2002**, *89*, 157602.
- (48) Souza, I.; Íñiguez, J.; Vanderbilt, D. First-Principles Approach to Insulators in Finite Electric Fields. *Phys. Rev. Lett.* **2002**, *89*, 117602.
- (49) Qin, G.; Qin, Z.; Yue, S.; Yan, Q.-B.; Hu, M. External electric field driving the ultra-low thermal conductivity of silicene. *Nanoscale* **2017**, *9*, 7227.
- (50) Yang, Z.; Yuan, K.; Meng, J.; Hu, M. Electric field tuned anisotropic to isotropic thermal transport transition in monolayer borophene without altering its atomic structure. *Nanoscale* **2020**, *12*, 19178.
- (51) Ding, W.; Zhu, J.; Wang, Z.; Gao, Y.; Xiao, D.; Gu, Y.; Zhang, Z.; Zhu, W. Prediction of intrinsic two-dimensional ferroelectrics in In2Se3 and other III2-VI3 van der Waals materials. *Nat. Commun.* **2017**, *8*, 14956.
- (52) Kong, B. D.; Paul, S.; Nardelli, M. B.; Kim, K. W. First-principles analysis of lattice thermal conductivity in monolayer and bilayer graphene. *Phys. Rev. B* **2009**, *80*, 033406.
- (53) Quan, Y.; Yue, S.-Y.; Liao, B. Electric field effect on the thermal conductivity of wurtzite GaN. *Appl. Phys. Lett.* **2021**, *118*, 162110.
- (54) Wee, D.; Kozinsky, B.; Marzari, N.; Fornari, M. Effects of filling in CoSb<sub>3</sub>: Local structure, band gap, and phonons from first principles. *Phys. Rev. B* **2010**, *81*, 045204.
- (55) Wang, C.; Guo, J.; Dong, L.; Aiyiti, A.; Xu, X.; Li, B. Superior thermal conductivity in suspended bilayer hexagonal boron nitride. *Sci. Rep.* **2016**, *6*, 25334.
- (56) Deng, S.; Yuan, J.; Lin, Y.; Yu, X.; Ma, D.; Huang, Y.; Ji, R.; Zhang, G.; Yang, N. Electric-field-induced modulation of thermal conductivity in poly(vinylidene fluoride). *Nano Energy* **2021**, *82*, 105749.
- (57) Yasuda, K.; Wang, X.; Watanabe, K.; Taniguchi, T.; Jarillo-Herrero, P. Stacking-engineered ferroelectricity in bilayer boron nitride. *Science* **2021**, *372*, 1458.
- (58) Balandin, A. A. Thermal properties of graphene and nanostructured carbon materials. *Nat. Mater.* **2011**, *10*, 569–581.
- (59) Togo, A.; Chaput, L.; Tanaka, I. Distributions of phonon lifetimes in Brillouin zones. *Phys. Rev. B* **2015**, *91*, 094306.
- (60) Machida, Y.; Matsumoto, N.; Isono, T.; Behnia, K. Phonon hydrodynamics and ultrahigh-room-temperature thermal conductivity in thin graphite. *Science* **2020**, *367*, 309–312.
- (61) Machida, Y.; Subedi, A.; Akiba, K.; Miyake, A.; Tokunaga, M.; Akahama, Y.; Izawa, K.; Behnia, K. Observation of Poiseuille flow of phonons in black phosphorus. *Sci. Adv.* **2018**, *4*, No. eaat3374.
- (62) Kolobov, A. V.; Fons, P.; Tominaga, J.; Ovshinsky, S. R. Vacancy-mediated three-center four-electron bonds in GeTe-Sb2Te3phase-change memory alloys. *Phys. Rev. B* **2013**, 87, 165206.
- (63) Wang, X.-P.; Li, X.-B.; Chen, N.-K.; Zhao, J.-H.; Chen, Q.-D.; Sun, H.-B. Electric field analyses on monolayer semiconductors: the example of InSe. *Phys. Chem. Chem. Phys.* **2018**, *20*, 6945–6950.
- (64) Shi, M. W.; Thomas, S. P.; Hathwar, V. R.; Edwards, A. J.; Piltz, R. O.; Jayatilaka, D.; Koutsantonis, G. A.; Overgaard, J.; Nishibori, E.; Iversen, B. B.; Spackman, M. A. Measurement of Electric Fields Experienced by Urea Guest Molecules in the 18-Crown-6/Urea (1:5) Host-Guest Complex: An Experimental Reference Point for Electric-Field-Assisted Catalysis. J. Am. Chem. Soc. 2019, 141, 3965–3976.
- (65) Hans, M.; Schneider, J. M. Electric field strength-dependent accuracy of TiAlN thin film composition measurements by laser-assisted atom probe tomography. *New J. Phys.* **2020**, *22*, 033036.
- (66) Foley, B. M.; Wallace, M.; Gaskins, J. T.; Paisley, E. A.; Johnson-Wilke, R. L.; Kim, J.-W.; Ryan, P. J.; Trolier-McKinstry, S.; Hopkins, P. E.; Ihlefeld, J. F. Voltage-Controlled Bistable Thermal Conductivity in Suspended Ferroelectric Thin-Film Membranes. *ACS Appl. Mater. Interfaces* **2018**, *10*, 25493–25501.

(67) Ning, S.; Huberman, S. C.; Zhang, C.; Zhang, Z.; Chen, G.; Ross, C. A. Dependence of the Thermal Conductivity of BiFeO<sub>3</sub> Thin Films on Polarization and Structure. *Phys. Rev. Appl.* **2017**, *8*, 054049. (68) Aryana, K.; Tomko, J. A.; Gao, R.; Hoglund, E. R.; Mimura, T.; Makarem, S.; Salanova, A.; Hoque, M. S. B.; Pfeifer, T. W.; Olson, D. H.; Braun, J. L.; Nag, J.; Read, J. C.; Howe, J. M.; Opila, E. J.; Martin, L. W.; Ihlefeld, J. F.; Hopkins, P. E. Observation of solid-state bidirectional thermal conductivity switching in antiferroelectric lead zirconate (PbZrO3). *Nat. Commun.* **2022**, *13*, 1573.